How to measure the Mueller matrix of liquid-crystal cells

Ingolf Dahl

Liquid Crystal Group, Department of Microelectronics and Nanoscience,
Chalmers University of Technology, S-412 96 Göteborg, Sweden

E-mail: f9aid@fy.chalmers.se

Abstract

The Mueller matrix is the transfer matrix in the Stokes algebra that describes the polarization of natural light. This matrix is very versatile for the task of characterizing the optical properties of liquid-crystal cells, since it can be used for comparison with theoretical calculations, the determination of material parameters and the modelling of the cell as an optical building block for technological use. We have constructed a Mueller-matrix spectrometer, with the ability to perform fast, dynamic measurements of the Mueller matrix of small areas of liquid-crystal cells throughout the visible range. To illustrate the potential of the instrument, dynamic measurements on a ferroelectric-liquid-crystal cell are presented and analysed. The optical measurements indicate that there is an asymmetry between the up and the down state, tilted smectic layers and polarization reversal initiated at the boundaries.

Keywords: Mueller matrix, liquid crystal, ferroelectric, Stokes vector, polarization, spectrometer, spectrograph, xenon lamp, photodiode array, visible range, retardation plates

1. Introduction

When we are working with optical devices which interact with the polarization of light, we need adequate mathematical tools. We then have the choice between the Jones [1] and the Stokes [2] algebra for the description of the polarization. The Jones algebra is adequate for coherent and monochromatic light, whereas the Stokes algebra is better for natural light, which mostly is incoherent, polychromatic and unpolarized. If we have complete knowledge about the light, we have only polarized light. However, our detectors and our eyes have limited spatial resolution, limited wavelength resolution and limited time resolution and frequency resolution. Fast variations cannot be resolved, so we see only an incoherent and unpolarized average. (Compare this with the concept of entropy and 'coarse-graining'!) The Stokes algebra can describe partially polarized and unpolarized light. Thus, the Stokes algebra is the correct algebra for most polarizing optical devices that interact with the colour of light, in the way it is experienced by human beings. In this algebra, we can use a matrix, *the Mueller matrix*, to characterize the transmission (or reflection) of a device for light at some wavelength and with arbitrary polarization. The Mueller matrix description allows us to separate those properties that depend on the orientation of the device from those that are independent of the orientation. This is useful in the comparison between experimental and theoretical descriptions and in the computer modelling of optical devices which are composites of several polarizing devices. We will recapitulate and give a short introduction to the necessary mathematical concepts and notation.

We describe the construction of a Mueller matrix spectrometer, which is suitable for liquid-crystal research. Liquid crystals are optically a bit special, since the polarization properties can vary fast both temporally and spatially and as a function of temperature. Often the sample is not freely rotatable, as usually is the case with mineral samples. Moreover, the geometrical configuration inside a liquid-crystal cell is a continuous function which cannot be characterized by a single variable. Thus, to characterize the liquid crystal, it is not sufficient to measure one or two single parameters,
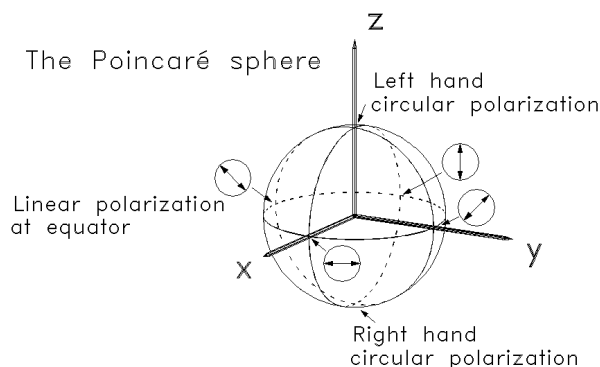
The Poincaré sphere

Left hand
circular polarization

Linear polarization
at equator

Right hand
circular polarization

Figure 1. The Poincaré sphere. Each point at the surface of the sphere represents one polarization state for fully polarized light. The points at the equator represent linear polarization, the poles represent circular polarization and all other points represent elliptical polarization.

or one or two components of the Mueller matrix. We need and can make use of the full information. For a liquid-crystal cell, measurement of the Mueller matrix will give us specific information about the internal geometrical configuration of the cell.

Our Mueller matrix spectrometer is able to measure the Mueller matrix for a small area of a liquid-crystal cell in the visible range. The illumination of the cell can be synchronized with the driving voltage of the cell, so that the (repetitive) switching process can be studied in detail, as a function of time.

We also describe a set of measurements on a ferroelectric liquid cell during switching, to illustrate the potential of this kind of measurement. The switching exhibited a non-trivial behaviour. We could indirectly determine the tilt of the smectic layers relative to the substrates by comparing the measurements with simple model calculations. This tilt determination usually requires x-ray measurements [3]. The tilt seems to force the molecules to switch on one side of the smectic cone. Asymmetries between the up state and the down state were found. It was also possible to verify that the boundary layers switched before the bulk of the liquid crystal did.

2. The theoretical background

2.1. The Stokes algebra

According to Stokes [2], general light could be seen as the sum of one unpolarized part and one fully polarized part. For unpolarized light, one parameter is needed to describe the intensity. For polarized light three intensity parameters are needed, so altogether four parameters are needed. These parameters should be chosen in an additive way. In our case, this means that they should be additive for incoherent sources of light. Then standard linear algebra could be applied. We thus define a *Stokes vector* with four parameters I, M, C and S, for light propagating in the z direction, where I is the total intensity, M is the difference in intensity for a polarizer along the x-axis and one along the y-axis, C is the difference in intensity for polarizers set at $\pm 45°$ to the x-axis and S is the

difference in intensity between left-handed and right-handed polarized light. These Stokes parameters could be written as a 4-vector:

$$\begin{pmatrix} I \\ M \\ C \\ S \end{pmatrix}. \tag{1}$$

2.2. The Poincaré sphere

Assume that the light is composed of two parts, one unpolarized with intensity I_u and one fully polarized with intensity I_p. The polarization of polarized light can be uniquely described by a point on the Poincaré sphere with unit radius (see [4] and figure 1), with the coordinates x, y and z. The Poincaré sphere can give a visual and intuitive picture of the action of different polarization components. We can now identify the Stokes parameters with the Poincaré sphere coordinates in the following way:

$$I \equiv I_u + I_p$$

$$M \equiv I_p x$$

$$C \equiv I_p y$$

$$S \equiv I_p z. \tag{2}$$

2.3. The Mueller matrix

An arbitrary optical-polarization component could be described by a 4×4 matrix, connecting the Stokes vector for the entering light with the Stokes vector for the transmitted light:

$$\begin{pmatrix} I \\ M \\ C \\ S \end{pmatrix}_{out} = A \begin{pmatrix} I \\ M \\ C \\ S \end{pmatrix}_{in} \tag{3}$$

where A is a 4×4 matrix, denoted *the Mueller matrix*, characterizing the component. Let A_{ij} be the matrix elements of the Mueller matrix. It is convenient to let the indices of the elements of the Mueller matrix and related matrices run from zero to three. A good reference article about polarimetry and the Mueller matrix has been written by Chipman [5].

The general Mueller matrix can be seen as a product PHU of three real matrices P, H and U, with different mathematical properties and different physical interpretations. P is a symmetrical matrix, representing a general partial-polarizing component. H represents a general depolarizing component. U is an orthogonal matrix and represents a generalized retarder. This factorization has been shown earlier by Lu and Chipman [6]. We can obtain alternative factorizations of the Mueller matrix by forming all possible permutations of P, H and U. Which permutation to choose is a matter of taste.

2.4. The polarizing part of the Mueller matrix

The general partial polarizer P, a *diattenuator*, is given by the following 4×4 matrix (see [6]):

$$P = \frac{1}{1+w} \begin{pmatrix} 1 & w\boldsymbol{n}^{\dagger} \\ w\boldsymbol{n} & M_D \end{pmatrix}$$
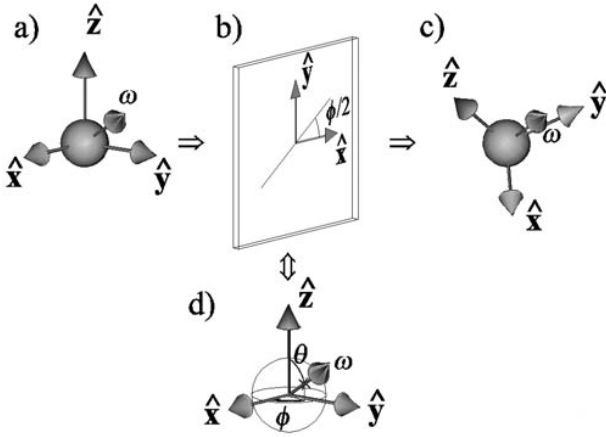
Figure 2. The fixed-point axis for a generalized retarder: (*a*) the Poincaré sphere of the incoming light, (*b*) a retardation plate with a local reference frame in real space and (*c*) the Poincaré sphere for the transmitted light. The action of the retarder plate is to rotate the Poincaré sphere around a fixed-point axis ω, characterized by a latitude angle θ and a longitude (azimuthal) angle ϕ, see (*d*). For the retarder plate, one of the directions of vibration in the retarder is inclined with the angle $\phi/2$ relative to the x-axis in real space.

where

$$M_D = (1 - w^2)^{1/2} \begin{pmatrix} 1 & 0 & 0 \\ 0 & 1 & 0 \\ 0 & 0 & 1 \end{pmatrix}$$
$$+ [1 - (1 - w^2)^{1/2}] \begin{pmatrix} n_x^2 & n_x n_y & n_x n_z \\ n_x n_y & n_y^2 & n_y n_z \\ n_x n_z & n_y n_z & n_z^2 \end{pmatrix} \quad (4)$$

and † denotes the transpose of the matrix, $n = \{n_x, n_y, n_z\}$ represents a unit vector and w is a weight factor, *the polarization weight*, between zero and unity.

2.5. The retarder part U of the Mueller matrix

The matrix U can be seen as a rotation of the Poincaré sphere around a *fixed-point axis* directed along the unit vector $\omega = \{\omega_x, \omega_y, \omega_z\} = \{\cos\phi \sin\theta, \sin\phi \sin\theta, \cos\theta\}$. The rotation angle is the *retardation angle* δ. We denote θ the *latitude angle* and ϕ the *longitude angle*, see figure 2.

Then the matrix U can be written in the most general way as

$$U = \begin{pmatrix} 1 & 0 \\ 0 & \omega_x^2(1 - \cos\delta) + \cos\delta \\ 0 & \omega_x\omega_y(1 - \cos\delta) + \omega_z \sin\delta \\ 0 & \omega_x\omega_z(1 - \cos\delta) - \omega_y \sin\delta \end{pmatrix}$$
$$\begin{matrix} 0 \\ \omega_x\omega_y(1 - \cos\delta) - \omega_z \sin\delta \\ \omega_y^2(1 - \cos\delta) + \cos\delta \\ \omega_y\omega_z(1 - \cos\delta) + \omega_x \sin\delta \end{matrix}$$
$$\left.\begin{matrix} 0 \\ \omega_x\omega_z(1 - \cos\delta) + \omega_y \sin\delta \\ \omega_y\omega_z(1 - \cos\delta) - \omega_x \sin\delta \\ \omega_z^2(1 - \cos\delta) + \cos\delta \end{matrix}\right). \quad (5)$$

We can see this component as a generalized retardation plate. A single simple ordinary optical retarder will rotate the Poincaré sphere around a fixed-point axis parallel to the equatorial plane and will thus have $\omega_z = 0$ and the angle θ equal to 90°. In

the general case the fixed-point axis could have any direction. The direction of the fixed-point axis is linked to the sign of the retardation: we are allowed to change the signs of both at the same time.

Since the matrix U is orthogonal, it will have four eigenvalues, all with absolute value unity. We will get two eigenvalues of unit value, with one eigenvector corresponding to unpolarized light. The other eigenvector represents the rotation axis of the Poincaré sphere. The third and fourth eigenvalues will form a complex-conjugate pair, with corresponding complex-conjugate eigenvectors. In unnormalized form the eigenvectors are given by

$\{1, 0, 0, 0\}$ (unpolarized light)
$\{0, \omega_x, \omega_y, \omega_z\}$ (the rotation axis)
$\{0, (-i\omega_y - \omega_x\omega_z), (i\omega_x - \omega_y\omega_z), \omega_x^2 + \omega_y^2\}$
     ($\{0, 1, -i\omega_z, 0\}$ if $\omega_x = \omega_y = 0$)
$\{0, (i\omega_y - \omega_x\omega_z), -(i\omega_x + \omega_y\omega_z), \omega_x^2 + \omega_y^2\}$
     ($\{0, 1, i\omega_z, 0\}$ if $\omega_x = \omega_y = 0$)   (6)

with the eigenvalues

$$1, 1, \cos\delta + i \sin\delta, \cos\delta - i \sin\delta. \quad (7)$$

2.6. The depolarization matrix H

The 4×4 depolarization matrix H can be written as a block matrix:

$$H = \begin{pmatrix} H_{00} & H_p^\dagger \\ \vec{0} & H_s \end{pmatrix} \quad (8)$$

where H_{00} is a constant, H_p is a three-component vector, $\vec{0}$ is a three-component zero vector and H_s is a 3×3 symmetrical matrix.

The matrix H contains contributions from two different depolarization mechanisms, one via the symmetrical matrix H_s and the other via the vector H_p. Here we will use the notation *matrix depolarization* and *vector depolarization* to differentiate between these mechanisms.

The symmetry of H_s implies that there exists a base in which H_s can be written as a diagonal matrix D_H. We can then write

$$H_s = U_H D_H U_H^\dagger \quad (9)$$

where U_H is a 3×3 orthogonal matrix, similar in shape to the lower right-hand corner of U. In the same way as with the matrix U, the determination of the matrix U_H can reveal characteristic directions in an experimental sample. We can see that, while U is uniquely determined from the Mueller matrix, there are 48 different ways to choose the order and sign of the eigenvectors of H_s if the eigenvalues are dissimilar and an infinite number of ways if two eigenvalues match. For an experimental Mueller matrix that depends on one continuous parameter, for instance time or wavelength, we could easily obtain discontinuities in U_H, if the algorithm for some reason jumps from one choice of order and sign to another. If the eigenvalues of H are almost degenerate, we also easily obtain huge but insignificant fluctuations in the locations of the eigenvectors.

It can sometimes be useful to have a single parameter that measures the ability of a component to depolarize light via

matrix depolarization. One orientation-independent choice of parameter is

$$k_D = \frac{H_{11} + H_{22} + H_{33}}{3H_{00}}. \tag{10}$$

For complete depolarization, this parameter is zero, whereas for no depolarization, it has the value unity. We will denote this parameter *the depolarization strength*. It also has a value in the case when the polarization weight is unity and it can be used as a quality criterion for polarizers and retarders. It can also be used to detect the presence of lateral variations in the geometrical configuration of a liquid-crystal cell: if different points in the sampled area have different retardation properties, the average effect will contain matrix depolarization.

To obtain vector depolarization, it is not enough to average over different retardation properties. We could instead obtain vector depolarization if we incoherently add light that has passed two differently oriented polarizers. Another way is to let the light pass first a polarizer and then an ideal depolarizer. In this way, we achieve pure vector depolarization. To characterize the vector depolarization we can write

$$H_p = H_{00} w_D n_D \tag{11}$$

where n_D is a normalized vector and w_D, denoted *the vector depolarization weight*, can take values between zero and unity.

Which parameters can we extract from P, H and U? The general Mueller matrix A is built up from 16 parameters. Three of these are needed for the description of the matrix P, ten for the description of H (H_{00} plus three parameters for H_p and six parameters for H_s) and the remaining three for the matrix U. From these parameters we can extract three different unit Poincaré-sphere vectors, one orthogonal vector set and seven scalar parameters.

2.7. The physical interpretation of Mueller matrix measurements on liquid-crystal cells

For simplicity, we discuss here only normal incidence of light on a liquid-crystal cell.

The most easily accessible parts of the Mueller matrix of a liquid-crystal cell are the retardation angle δ and the direction of the fixed-point axis, both of which are from the retarder part of the Mueller matrix. A uniform nematic cell is optically a retarder, with its slow vibration direction along the projection of the director on a surface parallel to the cell walls. A measurement of the longitude angle ϕ of the fixed-point axis could then provide us with most of the information we need to determine the director. The fixed-point axis will in this case be located on the equator of the Poincaré sphere and the angular position (longitude angle ϕ) will be independent of wavelength. In this way, we can also check whether the director is uniform. If we rotate the cell by an arbitrary angle, the measured longitude angle will be changed by double the amount, while the other parameters will be unaffected.

If instead we have a twist cell, for which the director is rotated progressively through the cell, then the fixed-point axis in the general case will be oblique, with a latitude angle which can take any value. In a way the reverse is also true: if the fixed-point axis is oblique or passes the poles of the Poincaré
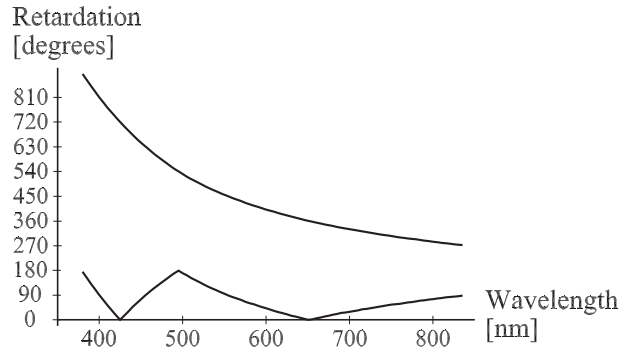

Figure 3. The lower jagged curve for the retardation could be transformed to the upper smooth curve by a proper choice of offsets and sign changes.

sphere, the sample being investigated must have some kind of twist or some other mirror asymmetry. Explicit formulae for twist-cell Mueller matrices have been calculated by Azzam [7]. This paper also contains explicit Mueller matrices for many other cases. For a uniform twist, numerical tests reveal that the latitude angle θ is strongly dependent on wavelength and that the longitude angle is constant.

If the fixed-point axis is located at the equator, with a longitude angle that is wavelength-dependent, this should indicate that there is a non-uniform but mirror-symmetrical director profile in the cell, for instance created by boundary layers. In the general case, without any symmetry, we could expect the longitude and latitude angles to vary with wavelength. It is often very useful to be able to check whether the symmetry of a theoretical model agrees with real cells; measurement of the Mueller matrix provides us with one method for performing such a check. If the symmetry agrees, we could proceed with a direct comparison of the experimentally obtained Mueller matrix and a numerical estimate from a theoretical model.

If we calculate or measure the Mueller matrix for a set of wavelengths and then calculate the retardation and the fixed-point axis, there is some arbitrariness in the choice of the sign of the fixed-point axis. This could give discontinuities or sharp corners in the curves for retardation and fixed-point axis angles, see figure 3. If we reverse the fixed-point axis, we should also reverse the sign of the retardation. With a given sign of the fixed-point axis, an arbitrary multiple of 2π can be added to the retardation angle. Often it is possible to choose the signs and phases in such a way that smooth curves are obtained. By extrapolation to zero retardation at infinite wavelength, it is often possible to obtain the absolute retardation at optical wavelengths. In some cases, the discontinuities cannot be eliminated. For instance, if the fixed-point axis passes smoothly through a pole, the longitude angle might change very fast. This can be seen as a defect of our representation of the spherical angles and has no physical significance. Another case of discontinuity is when the retardation is zero or a multiple of 2π. Then the direction of the fixed-point axis is undetermined and insignificant for the physics of the system.
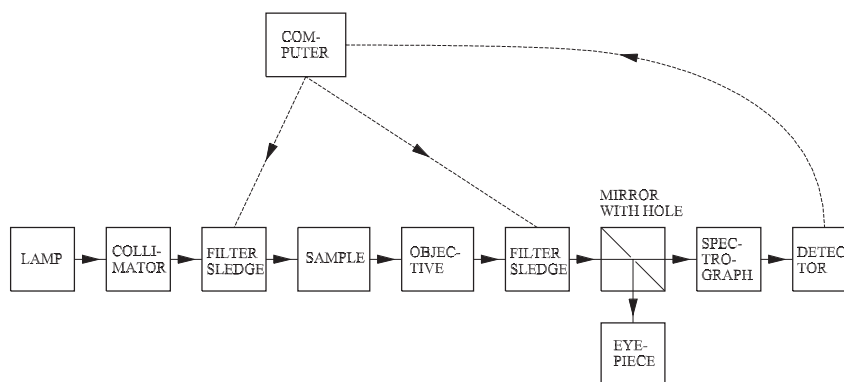
Figure 4. The block scheme for the Mueller matrix spectrometer.

3. Instrumental details

3.1. A Mueller matrix spectrometer

In order to obtain the Mueller matrix of real optical components, we have built a Mueller matrix spectrometer, whose operation is based on successive transmission measurements with 16 different filter combinations. With this instrument, we can characterize liquid-crystal cells and other planar optical components for all wavelengths in the visible range by finding the transmission Mueller matrix. During the measurement no presumptions about the optical behaviour are made; therefore, this set-up is best suited for large amplitude effects. For very small effects or very precise measurements, more specialized set-ups with more limited measurement ranges could be more appropriate. A block scheme for our instrument is shown in figure 4.

Using a xenon flash lamp as the light source, we can perform fast measurements of repetitive processes, synchronized with a switching voltage applied to a liquid-crystal cell. The main energy of the flash is emitted within 1 μs. The xenon flash lamp gives a very high light intensity confined to a small area, which allows measurements of small areas within the liquid-crystal cell (a round spot with diameter 160 μm). To obtain better statistics, typically 100 flashes are used for each filter setting in a measurement. At the other end of the light path there is an Oriel MS125 1/8 m Spectrograph with an InstaSpec photodiode array (PDA) detection system. With this, we could measure the intensity of the transmitted light with approximately 1 nm resolution in wavelength. In our measurements, we collect data for every fifth nanometre, which gives 92 different wavelengths within the visible and near-infrared range, from 380 to 835 nm. The reproducibility of the measured transmissions is typically within 1%. The parallelism of the sampling light is $\pm 2.5°$ at the liquid crystal. The polarization of the light is controlled by two Glan–Thompson prisms together with polarization-turning components on two step-motor-controlled filter sledges, one before the sample and one after the sample. By using translating filter sledges instead of rotating filter holders, we eliminate angular orientation errors. The polarizing components will be discussed more below. The xenon discharge arc illuminates a small aperture. The focusing optics forms a first image of the aperture inside the first Glan–Thompson prism and a second image at the sample.

An image of the sample is then formed at an inclined mirror with a small elliptical hole in it. By observation of the mirror through a microscope eyepiece, it is possible to check where in the sample the measurement is made. A circular image of the elliptical hole is then formed at the entrance slot of the spectrograph. The spectrograph finally maps the entrance slot on the PDA detector at the spectrograph exit in such a way that each detector element sees only one wavelength of light.

All the optical equipment is mounted on a 1500 mm Linos Photonics' FLS 95 Optical Rail, so the space required is one tabletop. Vibration damping and elimination of ambient light are not required. The optical components are arranged as modules according to the block scheme, such that each module is built on one or two FLS 95 carriers. 10 mm custom-made mounting plates have been used to mount standard components from the Linos Photonics Microbench on the carriers. In this way, the construction has been rendered compact and sturdy, while at the same time it has been possible to include the appropriate adjustment possibilities in the design, which was implemented in AutoCAD.

3.2. How to measure the Mueller matrix for a spectrum of different wavelengths

To measure the Mueller matrix of a transparent plate of some kind, we could, according to Stokes, perform transmission measurements for incoming unpolarized light, for horizontally polarized light, for linearly polarized light polarized 45° to the horizontal and for left-handed circularly polarized light. For each kind of incoming light we should perform four measurements of corresponding types of outgoing light, giving 16 measurements in total. Two things make this approach difficult in a situation in which we want to perform measurements at several wavelengths. In the experimental situation in which we want to use gratings to generate or analyse different wavelengths, it will be difficult to maintain the integrity of unpolarized light. We also have to find good achromatic retardation plates to generate the desired polarizations. To avoid the presence of unpolarized light, we suggest the use of four different types of fully polarized light instead of Stokes' choice and then one could perform a transformation of the experimental data to obtain the Mueller matrix. To obtain maximal experimental resolution, we should use four different polarizations, located at the corners of a regular tetrahedron inscribed in the Poincaré sphere. Two of

the points could be chosen at the equator, where they represent linear polarization along two different directions. The other two points represent right-handed and left-handed elliptical polarization. In spherical angles $\{\theta, \phi\}$ expressed in degrees, the tetrahedron points are given by $\{90, 0\}$, $\{90, 109.471\}$, $\{35.2644, -125.264\}$ and $\{144.736, -125.264\}$. We have chosen to combine cheap and simple polymeric sheet retarders to obtain approximately achromatic retardation plates. The drawback is then that the transformation matrices used for going from experimental data to the Mueller matrix representation become wavelength-dependent. The sheet retarders have a retardation that is of the 'zeroth-order' type, which means that the retardation for a typical $\lambda/2$ plate varies smoothly from $141°$ at 780 nm to $255°$ at 380 nm. Two or three such plates can be combined in such a way that the combination is less wavelength-dependent than are the individual elements [8, 9]. To explicitly define the position of these filters, we define a right-handed coordinate system for the experimental set-up, with the x-axis vertical and the z-axis along the direction of the light beam. The second Glan–Thompson prism is oriented to transmit light with vertical polarization. The second filter sledge has one filter position for each tetrahedron point. The first filter position is empty. The second filter position contains two $\lambda/2$ plates, oriented with their fast axes at the polar angles $13.68°$ and $41.05°$. The third filter position contains two $\lambda/2$ plates followed by one $\lambda/4$ plate, at angles $-15.00°$, $-32.63°$ and $-62.63°$. The fourth filter position contains the same set of retardation plates as the third filter position, but with components rotated by $90°$. The first Glan–Thompson prism and the filters in the first filter sledge are mounted to give maximum transmission when they are combined with the corresponding component in the second filter sledge. The first Glan–Thomson prism is thus also oriented to transmit vertical polarization. The spectrum obtained for parallel Glan–Thompson prisms, without any other polarizing or birefringent elements in the light path, can be used for the normalization of the other spectra.

Suppose that we make a measurement of an optical component, measuring the transmission for all of the 16 different combinations of filter positions. We collect the measured values in a matrix R_{ij}, where the first index i corresponds to the position in the first filter sledge and the second index j corresponds to the position in the second filter sledge. We can normalize R_{ij} in such a way that parallel Glan–Thompson prisms give a transmission of unity. In terms of the Mueller matrix A of the optical component and the Mueller matrices $A_{(1i)}$ and $A_{(2j)}$ of the filters in the filter sledges, the matrix R_{ij} can be written as

$$R_{ij} = \frac{1}{2} \begin{pmatrix} 1 & 1 & 0 & 0 \end{pmatrix} A_{(2j)} A A_{(1i)} \begin{pmatrix} 1 \\ 1 \\ 0 \\ 0 \end{pmatrix}. \quad (12)$$

This gives a set of 16 equations, one for each choice of input filter i and output filter j. We can rearrange these 16 equations as one matrix equation by writing

$$2R^{\dagger} = G_2 A G_1 \quad (13)$$

where G_1 and G_2 are two 4×4 matrices. Each column in G_1 characterizes one filter in the first filter set and each row of G_2

characterizes one filter in the second filter set. Since the first filter position in each filter set is empty, the first column of G_1 will contain the elements 1, 1, 0 and 0, whereas the first row of G_2 will contain the elements 1, 1, 0 and 0. If we know G_1 and G_2 for each wavelength, we can easily calculate the Mueller matrix A of the optical component.

3.3. Calibration of the filter sets

The matrices G_1 and G_2 each contain 12 variables, which we need to determine in order to be able to evaluate the measurements. If we had a calibrated Mueller matrix instrument, we could easily measure the properties of the filter. However, how should we calibrate an instrument if we have no sister instrument available? It is not sufficient to measure the properties of the set-up without any optical component inserted, since that will only give 16 constants from which to determine 24 variables. If we also measure the properties of an optical component (i.e. a retardation plate), we add 16 unknown variables and gain 16 measurement values. We have then 40 variables and 32 measurements, still too few measurements. To add more measurements, we can rotate the optical component by a known angle and repeat the measurement, since we know how the Mueller matrix is transformed by a rotation. We have used three angular positions, $45°$ apart, of a retardation plate, to obtain 64 measurement values in total, which should be enough to determine the values of the 40 variables. Then the problem is over-specified, so we can rewrite it as a minimization problem, wherein we minimize an error function with respect to the 40 variables. If we define a function named 'Squaresum' of a matrix as the sum of the squares of the elements, we can define both an input error f_i for a measurement as

$$f_i = \text{Squaresum}(R^{\dagger} - G_2 A G_1 / 2) \quad (14)$$

and an output error f_o as

$$f_o = \text{Squaresum}(A - 2G_2^{-1} R^{\dagger} G_1^{-1}). \quad (15)$$

To make the variables converge to physically reasonable values, we can minimize the sum of the input and output errors for the measurements. We denote the 40 variables g_1 to g_{24} and m_{00} to m_{33} and let

$$G_1 = \begin{pmatrix} 1 & g_1 & g_5 & g_9 \\ 1 & g_2 & g_6 & g_{10} \\ 0 & g_3 & g_7 & g_{11} \\ 0 & g_4 & g_8 & g_{12} \end{pmatrix}$$

$$G_2 = \begin{pmatrix} 1 & 1 & 0 & 0 \\ g_{13} & g_{14} & g_{15} & g_{16} \\ g_{17} & g_{18} & g_{19} & g_{20} \\ g_{21} & g_{22} & g_{23} & g_{24} \end{pmatrix} \quad (16)$$

and let the Mueller matrix of the optical component be defined by

$$A = \begin{pmatrix} m_{00} & m_{01} & m_{02} & m_{03} \\ m_{10} & m_{11} & m_{12} & m_{13} \\ m_{20} & m_{21} & m_{22} & m_{23} \\ m_{30} & m_{31} & m_{32} & m_{33} \end{pmatrix}. \quad (17)$$

We know that there are some physical limits on the possible values of these 40 variables and, to find a proper minimum, we

can add some positive 'penalty' functions if the variables go outside the physical limits during the minimization. We have the following inequalities for the variables g_1 to g_{24}:

$$(g_2^2 + g_3^2 + g_4^2)^{1/2} \leqslant g_1 \leqslant 1$$
$$(g_6^2 + g_7^2 + g_8^2)^{1/2} \leqslant g_5 \leqslant 1$$
$$(g_{10}^2 + g_{11}^2 + g_{12}^2)^{1/2} \leqslant g_9 \leqslant 1$$
$$(g_{14}^2 + g_{15}^2 + g_{16}^2)^{1/2} \leqslant g_{13} \leqslant 1$$
$$(g_{18}^2 + g_{19}^2 + g_{20}^2)^{1/2} \leqslant g_{17} \leqslant 1$$
$$(g_{22}^2 + g_{23}^2 + g_{24}^2)^{1/2} \leqslant g_{21} \leqslant 1. \quad (18)$$

The elements of a physically realizable Mueller matrix are subject to the following restrictions, derived by Givens and Kostinski [10] and Gil [11].

(i) Let G be the diagonal matrix with the diagonal elements $(1, -1, -1, -1)$. Then the eigenvalues of $GA^{\dagger}GA$ should be real, and the eigenvector (s_0, s_1, s_2, s_3) corresponding to the largest eigenvalue should be a possible Stokes vector, so that the polarization $\rho = (s_1^2 + s_2^2 + s_3^2)^{1/2}/s_0 \leqslant 1$. Then the Mueller matrix maps Stokes vectors onto Stokes vectors.

(ii) For a passive optical device, we require that the intensity of any Stokes vector should not increase, which leads to the conditions

$$(m_{01}^2 + m_{02}^2 + m_{03}^2)^{1/2} \leqslant m_{00} \leqslant 1$$
$$- (m_{01}^2 + m_{02}^2 + m_{03}^2)^{1/2}. \quad (19)$$

(iii) An optical component, which can be seen as an average over pure Mueller matrices (without depolarization), is subject to the following restriction [11]:

$$m_{00} \leqslant 1 - (m_{10}^2 + m_{20}^2 + m_{30}^2)^{1/2}. \quad (20)$$

As a penalty function, to force the variables back to physical reality, we can choose

$$f(x) = \begin{bmatrix} 0 \text{ for } x \leqslant 0 \\ \sqrt{x} \text{ for } x > 0 \end{bmatrix}. \quad (21)$$

This function has the benefit of having an infinite derivative at $x = 0+$, which means that the penalty function has a reasonable chance of keeping the variables inside the physical limits, even if the function to be minimized has a finite slope outside the allowed region. If we still found a minimum outside the physical limits, we could increase the strength of the penalty, by multiplying the penalty function by a constant factor, and perform a new optimization. The penalty function for the first inequality in (18) can be chosen as

$$f(g_2^2 + g_3^2 + g_4^2 - g_1^2). \quad (22)$$

Similar penalty functions can be chosen for the other inequalities. The input and output error functions and suitable penalty functions can be added to obtain a 'cost function', which can be minimized to find appropriate values for the variables g_1 to g_{24} and m_{00} to m_{33} for each wavelength. Finding the minimum for each wavelength of the cost function with respect to 40 variables would have exceeded any computer time account a few years ago, but now it is possible to approach the optimal values in finite time on a PC. After minimization of the cost function, we seem to get a reliable calibration of the filters from the wavelength 410 nm and upwards. Below 410 nm, the transmission of the filters is low and the matrices involved become ill conditioned.
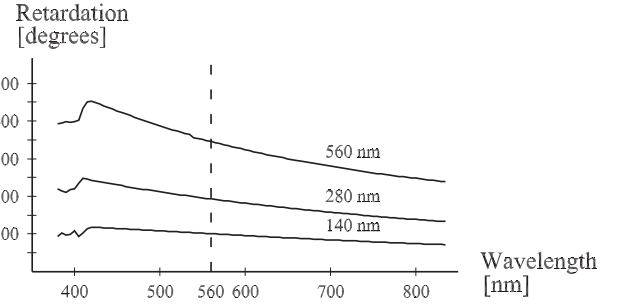
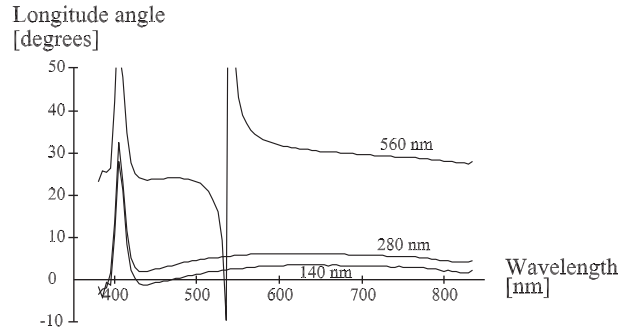**Figure 5.** Retardation angles for the three retardation plates.

Figure 6. The longitude angles as functions of wavelength for the three retarders.

4. Experimental details

4.1. Measurements on retardation plates

As an example of an application of the Mueller matrix spectrometer, we have measured the properties of Polaroid optical retarders with nominal retardations 140 ± 20, 280 ± 20 and 560 ± 25 nm. The nominal values of the retardations should be valid for light with the wavelength 560 nm, but, due to the physical properties of the polymer material, these values for nominal retardation are approximately valid over a wide wavelength range. To obtain the retardation in degrees, we should multiply the nominal retardation by 360 and divide by the wavelength in nanometres. These optical retarders are delivered as transparent plastic sheets, similar in appearance to polarizing film. They have been used in the filters in the filter sledges in the Mueller matrix spectrometer.

The measured retardations of the three retardation plates are shown in figure 5. The retardations at the wavelength 560 nm have been measured to be $101°$, $187°$ and $346°$, which correspond to 156, 291 and 538 nm.

The angular position on the Poincaré sphere of the fast vibration direction can also be determined. The latitude angle for each of the three plates is very near $90°$, as it should be for retardation plates. The longitude angles are shown in figure 6. For the 560 nm plate, the retardation passes $360°$ at the wavelength 538 nm and, at that wavelength, the angular position of the fast vibration direction is arbitrary. Therefore, one could expect discontinuities in the measured position of the vibration direction at this wavelength.

The orthogonal matrix U is the most significant part of the Mueller matrix, so a discussion about the depolarizing and polarizing parts for these retardation plates would be too
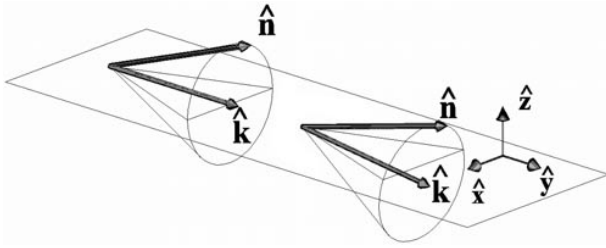
Figure 7. The geometry of the cell. The left-hand cone illustrates the case when the smectic layer normal $\hat{k}$ is parallel to the substrate. The right-hand cone corresponds to tilted smectic layers, with an angle of 7° between $\hat{k}$ and the substrate. The electrical field is parallel to $\hat{z}$.

technical and too uninteresting for the intended readers of this paper.

4.2. Measurements on ferroelectric-liquid-crystal cells

As another example to illustrate the potential of the Mueller matrix method, we have performed measurements on a ferroelectric-liquid-crystal cell in the smectic-C phase. In this phase the elongated molecules are locally aligned parallel and tilted relative to the smectic layer normal $\hat{k}$. At a specific temperature, the tilt angle is constant, but there are normally long-range distortions of the tilt direction. The local major axis of the optical index ellipsoid (the smectic-C $\hat{n}$-director) is parallel to the average local long axis of the molecules. Different wavelengths of light might see slightly different tilt angles of the molecules. At a specific temperature, all possible directions of the smectic-C $\hat{n}$-director form a cone around the layer normal. Often, the tilt direction is not constant throughout the cell. Instead it will form a continuous function of the spatial coordinates ('the geometrical configuration') and we do not know exactly what the continuous function for the tilt direction looks like. Thus, we cannot exactly predict the optical behaviour. Instead, we need to work in the reverse direction: we first measure the optical properties and then extract useful information that tells us something about the geometrical configuration. The cell of this study was of approximate thickness 1.9 μm, filled with the chiral smectic-C substance FELIX-014 from Hoechst. The cell was fabricated at the company FLC Optics AB, which was later incorporated into the company Radians Innova in Göteborg. The surface treatment was parallel rubbed polyimide, which should give an orientation with the smectic layer normal parallel or almost parallel to the substrate (bookshelf geometry, see figure 7). The cell was initially 'activated' by application of a ±20 V square wave voltage for some few seconds. The measurement was performed at room temperature (22 °C). The cell was oriented in such a way that a fixed-point axis along the smectic layer normal would have a longitude angle of 180°. This longitude angle is directly connected to the projection of the smectic-C $\hat{n}$-director onto the substrate plane: a rotation of the $\hat{n}$-director by some angle around the substrate normal will change the longitude angle by double the amount (cf figure 2).

To the cell we applied alternating positive and negative pulses, each pulse being followed by a holding voltage of the same sign, see figure 8. The repetition frequency was 20 Hz. The pulse length τ_p was 25 or 75 μs, the pulse height
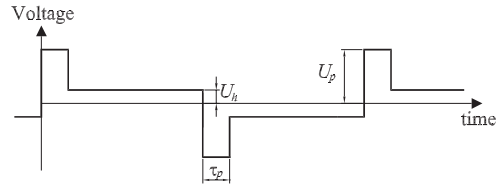

Figure 8. The waveform of the applied voltage. The figure is not drawn to scale: the pulse length τ_p is 25 or 75 μs, while the repetition period is 50 ms. The pulse height U_p is ±15 or ±30 V, while the holding voltage U_h is 0, ±0.5 or ±1.0 V.

U_p was ±15 or ±30 V and the holding voltage U_h was 0, ±0.5 or ±1 V. This provides twelve different combinations of pulse length, pulse height and holding voltage. For each such combination, Mueller matrix measurements have been performed at the following time positions in microseconds, measured relative to the start of the switch-down pulse: −50, 0, 5, 10, 20, 30, 60, 100, 200, 400, 1000, 2000, 4000, 8000, 16000, 24000, 24950, 25000, 25005, 25010, 25020, 25030, 25060, 25100, 25200, 25400, 26000, 27000, 29000, 33000, 41000 and 49000.

This gives 32 different time positions. Since the duration of the flash is approximately 1 μs, we obtained dynamic information about the switching behaviour. In each measurement the 16 components of the Mueller matrix have been measured at 92 different wavelengths, so we ended up with $12 \times 32 \times 92 \times 16 = 565248$ numbers in total, which of course represent more data than it is possible to comprehend. To understand anything from the measurements we have extracted the general features. If not stated otherwise, experimental values below are measured at the wavelength 600 nm.

4.2.1. Essentially one up and one down state.
First, we can see that the longitude angle of the fixed-point axis for light of wavelength 600 nm switches from an angle near 138° to an angle near 223° for all members of the series, except for the case of incomplete switching when τ_p was 25 μs and the pulse height U_p was ±15 V. In this case, when the holding voltage U_h was 0 V, the longitude angle varies between 140° and 197°, with relaxation to a longitude angle of 147° both after the positive pulse and after the negative pulse. The holding voltage of ±0.5 V gives a longitude angle between 141° and 180°, with slow unfinished relaxation towards two different states after the up pulse and the down pulse. The holding voltage ±1 V gives full switching between 141° and 220°, but the pulses are not strong enough to switch the cell completely and the longitude angle reaches the end positions by slow relaxation just before the next pulse. In a simple model, with uniform orientation and rigid motion of the $\hat{n}$-director, a swing of 85° of the fixed-point axis corresponds to movement around a cone with cone angle 21.25°.

4.2.2. A non-constant geometrical configuration.
If we compare the longitude angle of the fixed-point axis at different wavelengths, we see some dispersion. To obtain a numerical value for the dispersion of the longitude angle, we use the difference between the longitude angle at 700 nm and the longitude angle at 450 nm. For a uniformly oriented smectic-C liquid crystal, the direction of one principal dielectric axis
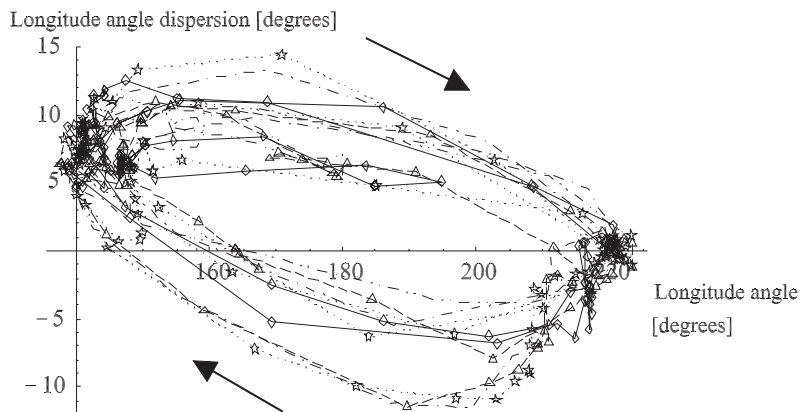
Figure 9. Longitude angle dispersion versus longitude angle (at 600 nm) for all members of the measurement series. The arrows show the time direction. This figure and also the next are intended to illustrate the spread of data and the general features common to all the different applied waveforms, rather than the less significant differences between the different waveforms.

agrees with the $\hat{n}$-director. The tilt angle between this direction and the smectic layer normal may depend on the wavelength of the light. If the liquid crystal in our cell is oriented uniformly, we should expect a linear relation between the longitude angle for a fixed wavelength and the wavelength dispersion of the longitude angle. This kind of dispersion we call *intrinsic dispersion*. However, the relation we see (see figure 9) is more complicated, with different signs of the dispersion during the up and down pulses. In some cases we can also see a slow relaxation between the pulses, which changes the dispersion while the longitude angle remains essentially constant. From this we conclude that there is a non-constant geometrical configuration, with variation along a direction orthogonal to the substrate plates. Moreover, the geometrical configuration during the up pulses is different from the configuration during the down pulses, even when the longitude angle is the same. Dispersion due to a non-constant geometrical configuration we call *configurational dispersion*.

A simple numerical simulation indicates that the liquid crystal near the substrates switches *before* the region in the middle of the sample.

4.2.3. Nearly optical mirror symmetry. When the geometrical configuration has mirror symmetry optically, the latitude angle of the fixed-point axis is 90°. On the other hand, for a twisted configuration with a definite sign, we would expect a latitude angle that is significantly different from 90°. We measure a latitude angle between 89° and 93°, which makes a strongly twisted configuration improbable. For our cell, we can thus rule out strong polar boundary conditions, which would give an optically twisted situation. We could also rule out the chevron SSFLC cell configuration proposed by Lagerwall *et al* [12], which displays a strong splaying of the polarization, implying a twist of the principal optical axes. There is a weak asymmetry of the latitude angle around the value 90°, which might imply weakly polar (chiral) boundary conditions, but that might be a measurement artefact.

4.2.4. The change in retardation is small: do we have tilted smectic layers? The measurements reveal a relation between the longitude angle and the retardation, see figure 10. The

retardation is largest about 5° from the extreme values of the longitude angle and smallest in the middle at the longitude 180°. We could try to model this behaviour by cone switching, assuming that the smectic layer normal $\hat{k}$ is parallel to the substrates and that the $\hat{n}$-director starts in the substrate plane and follows a cone path out of the substrate plane and back again. However, if we assume that there occurs a rigid movement (with constant configuration) of the $\hat{n}$-director and use reasonable values of the birefringence, we would get at least twice the change in retardation that we have measured. It is also difficult to get this low change in retardation by assuming that the behaviours of the boundary layers and the bulk layer differ.

If we assume the presence of tilted smectic layers, we could easily explain the general behaviour. With tilted layers, with $\hat{k}$ oblique to the substrate plane, the $\hat{n}$-director could move around the cone in two ways: either it begins by moving away from the substrate plane or it begins by moving towards the substrate plane. The measured change in retardation is consistent with a movement whereby the $\hat{n}$-director passes the substrate plane twice, with a layer tilt angle of approximately 7° between the smectic layer normal and the substrate plane. In figure 11 the retardation is drawn for two constant configurations: one with an angle of 6.6° between the smectic layer normal and the substrate plane and one with an angle of 8.8°. (The cone angle was assumed to be 21.22° for the 6.6° case and 21.12° for the 8.8° case. The thickness was assumed to be 1900 nm, the wavelength of light was assumed to be 600 nm, the ordinary refractive index was assumed to be 1.5 and the birefringence was assumed to be 0.15728.) Most of the experimental points are located in the neighbourhood of these curves. We have already found that we have to assume a non-constant geometrical configuration, but figure 10 indicates that the main feature is cone switching around one of the sides of a tilted cone. A careful study of figure 10 reveals a slight asymmetry between the rightmost and leftmost data points: lower values of retardation are reached on the left-hand side. This could indicate that there is a deformed configuration at the left-hand end.

To find the sign of the layer tilt and differentiate between uniform tilt and a chevron configuration, Mueller matrix measurements with oblique incidence of light could be used.
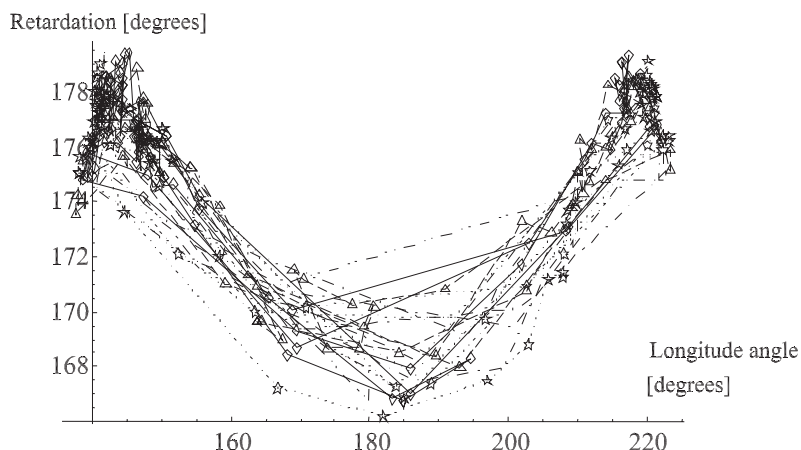
Retardation [degrees]

Figure 10. Retardation versus longitude angle (at 600 nm) for all members of the measurement series.
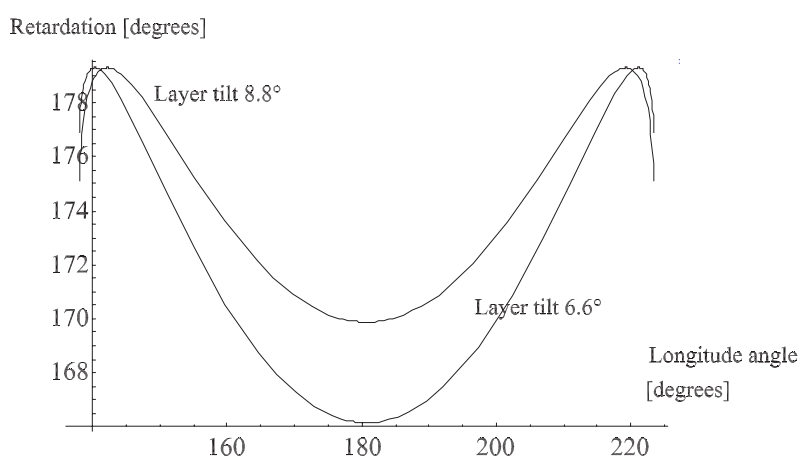
Retardation [degrees]

Figure 11. Calculated retardation versus longitude angle (at 600 nm) for two angles of layer tilt.

For the actual cell, such measurements have not been made, since the layer tilt was revealed first when the measurements were terminated.

4.2.5.   Break-up in domains during switching.   The depolarization weight is above 0.98 between the pulses, but starts to decrease immediately after the start of the pulses for the ±30 V pulses and sometimes falls as low as 0.93. This indicates that the liquid crystal breaks up in domains during the switching. The shape of the depolarization part of the Mueller matrix indicates that the different domains differ in their longitude angle, indicating that there is a varying delay time for the polarization switchover in different regions of the area. This time jitter could be due to small variations in the boundary conditions, since the time delay should be sensitive to such variations. There is no significant difference in the depolarization weight between switching up and switching down.

4.2.6.   The optical change is not solely due to movement of domain borders.   Imagine a situation in which we have 'up' domains and 'down' domains and the switching from the whole sample up to the whole sample down occurs via simple movements of the domain borders. In such a situation, the Mueller matrix of the intermediate states should be a

weighted sum of the Mueller matrices of the extreme positions. This would give a much lower depolarization strength than the measured value, so such a model cannot explain the measurements.

4.2.7. Fast relaxation after the pulses.   The longitude angle reaches its extreme values during the pulses. After the pulse, there is a fast relaxation towards a state with a longitude angle nearer 180°. One millisecond after the start of the pulse the relaxation is about 9° for zero holding voltage, about 5° for ±0.5 V holding voltage and about 2° for ±1 V holding voltage, all in the case of complete switching. In the case of incomplete switching, the relaxation is considerably larger. During this relaxation, the longitude angle dispersion is almost constant, while the retardation increases to its maximum value, which indicates that the $\hat{n}$-director becomes more parallel to the substrates.

4.2.8.   Very slow relaxation when switching is incomplete and when there is a holding voltage.   When the switching is incomplete and a holding voltage is present, there is a slow relaxation of the longitude angle towards the extreme values. For 1 V holding voltage the relaxation speed is around 3000° s^{-1} near the longitude angle 180°, whereas the relaxation during the 15 V pulses reaches values near

1947

$(10^6)^\circ$ s^{-1} at the same relaxation angle. The slow relaxation speed in the presence of the holding voltage implies the presence of ionic screening. Low values of the depolarization strength during the slow relaxation imply domain break-up and indicate that relaxation occurs by the movement of the domain borders.

4.2.9. Well-aligned states after the fast relaxation. If we study the retardation data, the maximum values of retardation are found approximately 5° above the minimum longitude angle and approximately 5° below the maximum longitude angle, at data points located in time after the fast relaxation after the pulses. At these points, the latitude angle is very near 90°, indicating that there is good mirror symmetry. We can conclude that the states reached after the fast relaxation are quite well aligned, but with the fixed-point axis a little bit away from the extreme values of the longitude angle. Some configurational dispersion remains and this dispersion seems to be more pronounced for the left-hand 'down' state, with longitude angle near 140°, than it is for the right-hand 'up' state, with longitude angle near 220°. This indicates that there is a small asymmetry between the 'down' state and the 'up' state. We can also see this asymmetry in the start-up time for switching. The time taken to reach the longitude angle 180° is usually much shorter when one starts from the 'up' state than it is when one starts from the 'down' state.

4.2.10. Measurements on the cell at rest also reveal an up–down asymmetry. Between the various measurement series, the cell was disconnected from the voltage source and Mueller matrix measurements were performed on the cell on ten occasions. Eight of these occasions gave retardation $176.4 \pm 1.1°$, longitude angle $146.2 \pm 0.5°$, latitude angle $90.8 \pm 0.6°$ and dispersion $9 \pm 1°$. These eight measurements seem to represent the same physical down state. Two of the measurements displayed a quite different behaviour with mirror asymmetry: retardation $168.4 \pm 1°$, longitude angle $209 \pm 1°$, latitude angle $80.1 \pm 1.1°$ and dispersion $-13.3 \pm 1.2°$. This asymmetry implies that some (unintentional) asymmetry was introduced during the cell preparation.

4.2.11. Are there fixed boundary conditions? One possible model for the geometrical configuration of the liquid crystal is to assume that there are fixed boundary conditions at the surfaces. It is difficult to interpret the measurements as indications of fixed boundary conditions.

4.2.12. A model for the switching behaviour. An exact model for the switching behaviour requires detailed mathematical simulation of the configuration and the optical properties, which would expand the scope of this paper too much. However, we can see what the starting points should be. With tilted smectic layers, the intersection between the smectic cone and the substrate planes defines two positions where the smectic-C $\hat{n}$-director is parallel to the substrates. In the 'up' state, the configuration seems to be constant and near one of these positions for the $\hat{n}$-director. However, this state does not seem to have long-term stability: when it is disconnected, it seems to relax to a twisted state with high dispersion and low retardation. This indicates that boundary conditions near at least one of the substrates gradually change. The 'down' state, which seems to be more stable, is deformed. Thus, the boundary conditions for the $\hat{n}$-director in the 'down' state cannot be exactly the same on both the substrates, and cannot be exactly in the other position parallel to the substrates.

Acknowledgments

References

[1] Jones R C 1975 A new calculus for the treatment of optical systems, eight papers published in J. Opt. Soc. Am. from 1941 to 1956 *Polarized Light* ed W Swindell (Dowden: Hutchingson and Ross)

[2] Stokes G G 1852 On the composition and resolution of streams of polarized light from different sources *Trans. Camb. Phil. Soc.* **9** 399–416

[3] Rieker T P *et al* 1987 'Chevron' local layer structure in surface-stabilized ferroelectric smectic-C cells *Phys. Rev. Lett.* **59** 2658–61

[4] Bigelow J E and Krashnow R A 1977 *Appl. Opt.* **16** 2090–6

[5] Chipman R A 1994 Polarimetry *Handbook of Optics* (New York: McGraw-Hill)

[6] Lu S-Y and Chipman R A 1996 Interpretation of Mueller matrices based on polar decomposition *J. Opt. Soc. Am.* A **13** 1106–13

[7] Azzam R M A 1978 *J. Opt. Soc. Am.* **68** 1756–67

[8] Andersson G *et al* 1989 Device physics of the soft-mode electro-optic effect *J. Appl. Phys.* **66** 4983–95

[9] Hariharan P and Ciddor P E 1997 Achromatic switchable polarization rotators *Opt. Eng.* **36** 952–6

[10] Givens C R and Kostinski A B 1993 A simple necessary and sufficient condition on physically realizable Mueller matrices *J. Mod. Opt.* **40** 471–81

[11] Gil J J 2000 Characteristic properties of Mueller matrices *J. Opt. Soc. Am.* A **17** 328–34

[12] Lagerwall S T *et al* 1989 Ferroelectric liquid crystals: the development of devices *Ferroelectrics* **94** 3–62